Multifunctional hollow nanoparticles based on graft-diblock copolymers for doxorubicin delivery

Pei-Lin Lu [a,1], Yi-Chun Chen [b,1], Ta-Wei Ou [c], Hung-Hao Chen [d], Hsieh-Chih Tsai [e], Chih-Jen Wen [a], Chun-Liang Lo [f,*], Shiaw-Pyng Wey [a,g], Kun-Ju Lin [a,g], Tzu-Chen Yen [a,g,**], Ging-Ho Hsiue [b,h,***]

[a] Department of Nuclear Medicine and Molecular Imaging Center, Chang Gung Memorial Hospital, Taoyuan, Taiwan 333, ROC
[b] Department of Chemical Engineering, National Tsing Hua University, Hsinchu, Taiwan 300, ROC
[c] Department of Chemical & Materials Engineering, National Central University, Taoyuan, Taiwan 320, ROC
[d] Department of Applied Chemistry, National Chiao Tun University, Hsinchu, Taiwan 300, ROC
[e] Graduate Institute of Engineering, National Taiwan University of Science and Technology, Taipei, Taiwan 106, ROC
[f] Department of Biomedical Engineering, National Yang Ming University, Taipei, Taiwan 112, ROC
[g] Department of Medical Imaging and Radiological Sciences, Graduate Institute of Medical Physics and Imaging Science, Chang Gung University, Taoyuan, Taiwan 333, ROC
[h] R&D Center for Membrane Technology, Chung Yuan Christian University, Chungli, Taiwan 320, ROC

ARTICLE INFO

ABSTRACT

This article reports a flexible hollow nanoparticles, self-assembling from poly(N-vinylimidazole-co-N-vinylpyrrolidone)-g-poly(D,L-lactide) graft copolymers and methoxyl/functionalized-PEG-PLA diblock copolymers, as an anticancer drug doxorubicin (Dox) carrier for cancer targeting, imaging, and cancer therapy. This multifunctional hollow nanoparticle exhibited a specific on-off switch drug release behavior, owning to the pH-sensitive structure of imidazole, to release Dox in acidic surroundings (intracellular endosomes) and to capsulate Dox in neutral surroundings (blood circulation or extracellular matrix). Imaging by SPECT/CT shows that nanoparticle conjugated with folic acids ensures a high intratumoral accumulation due to the folate-binding protein (FBP)-binding effect. In vivo tumor growth inhibition shows that nanoparticles exhibited excellent antitumor activity and a high rate of apoptosis in cancer cells. After 80-day treatment course of nanoparticles, it did not appreciably cause heart, liver and kidney damage by inactive Dox or polymeric materials. The results indicate that the flexible carriers with an on-off switched drug release may be allowed to accurately deliver to targeted tumors for cancer therapy.

© 2010 Elsevier Ltd. All rights reserved.

1. Introduction

For anticancer drug delivery systems, many systems have been discussed and exemplified regarding as traditional systems such as liposomes, polymer-based therapeutics, and inorganic particles. Polymer therapeutic is considered to be a potential candidate displaying well bioavailability and high molecular manipulation for use in cancer treatment. The term polymer therapeutics describes several distinct classes of agent, including polymer-drug conjugates [1,2], micelles [3,4], and mixed micelles [5,6] that have now entered clinical development because of their intrinsic physical properties and their abilities to target specific locations. Much research has recently been focused on the study of mixed micelles as drug carriers in the hunt for improved cancer therapy. The potential advantages of mixed micelles as potential drug carriers include 1) the fact that they can be degraded into nontoxic substances that may be readily excreted by the body; 2) the possibility of modulating the micellar structure to improve intracellular drug delivery; and 3) the possibility of modifying the polymers for in vivo cancer targeting and imaging. Despite such potential advantages, in vivo studies on mixed micelles as potential anticancer drug delivery systems remain scanty. The major problem that limits the wider application of mixed micelles as a drug carrier is the uncertainty about the structure of micelles during micellization in individual and mixed micellar systems.

We have recently shown that mixed micelles with a solid core and a flexible shell prepared by mixing a graft copolymer with one or more diblock copolymers have an individual micellar structure [7–9]. We were able to control the core-shell structure and the

particle size by varying the graft copolymer/diblock copolymer ratio. The core-shell structure and the micellar size are the two key parameters that need to be optimized for drug delivery applications in oncology. These factors govern the biodistribution and the intracellular uptake of drug carriers; of note, these parameters are highly dependent on the physical properties of the particles [10,11]. To further investigate the usefulness of mixed micelles for drug delivery applications in the field of oncology, we have developed a mixed micellar system involving multifunctional micelles (115 nm in size) containing doxorubicin (Dox) for cancer therapy, cy5.5 dye for *in vivo* imaging, and folic acid for targeting cancer cells [6]. According to preliminary results, the targeting ligand, folic acid, allowed the accumulation of the cytotoxic agent into tumor cells.

In the present study, we describe the preparation of hollow multifunctional three-compartment nanoparticles that contain 1) Dox as an anticancer drug; 2) a radiotracer, and 3) a targeting molecule (Fig. 1). This multifunctional nanoparticle system containing both a hollow core and a flexible shell may be considered as a platform for treating, imaging, and targeting tumors *in vivo*. Firstly, we have investigated the nanoparticle structure and drug release behavior of multifunctional hollow nanoparticles to clarify whether they would release the loaded drug in the intracellular acidic regions such as endosomes and lysosomes. Secondly, we conducted biodistribution studies of multifunctional hollow nanoparticles in mice and assessed the therapeutic effects of micelles on experimental tumors and the induction of apoptosis in cancer cells. We subsequently investigated the nanoparticle stability in the liver and experimental tumors. To evaluate the potential long-term cytotoxic effects, we finally examined the effects of nanoparticles on hepatic and renal function at 80 days postinjection.

2. Materials and methods

2.1. Synthesis of P(NVI-co-NVP)$_{9600}$-g-PLA$_{4900}$

First, PLA with an end-cap of methacrylated group (PLA-EMA, Mn 1630) was synthesized by ring-opening polymerization [7]. The graft copolymer, poly(NVI-co-NVP)-g-PLA was then synthesized by traditional free radical copolymerization.
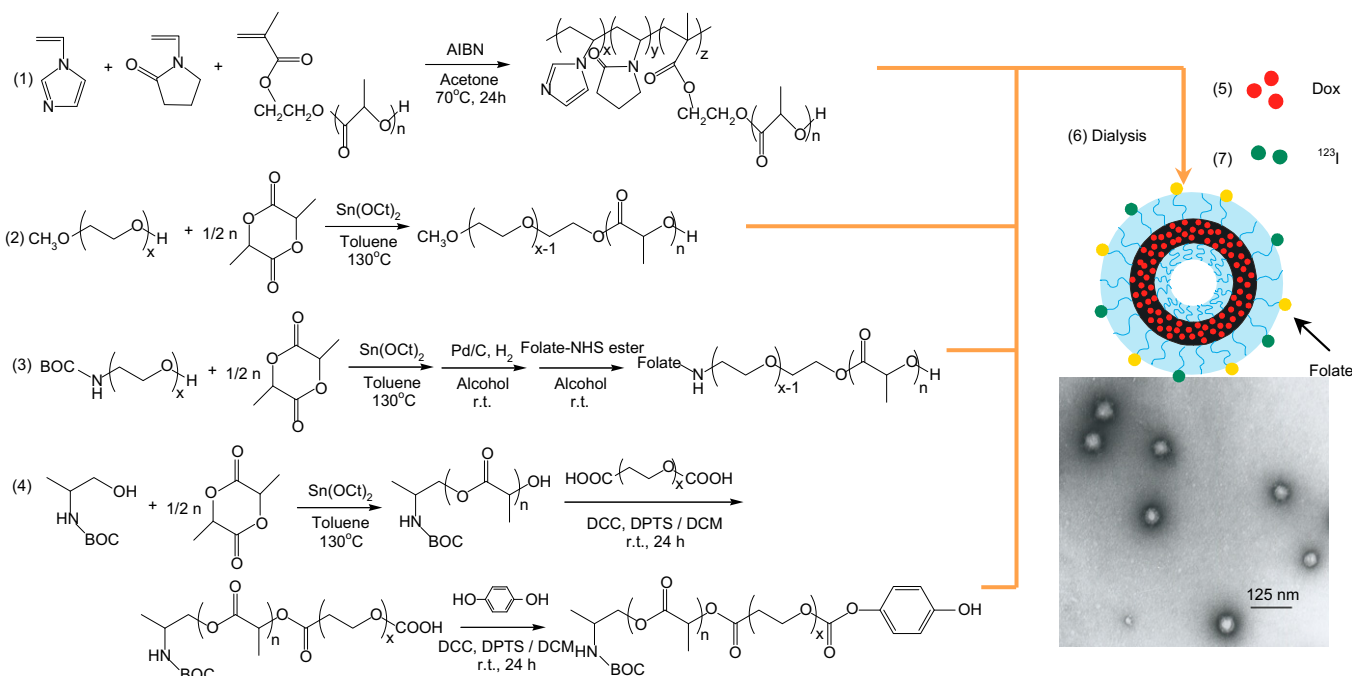
Briefly, PLA-EMA, NVI, NVP, and initiator AIBN were dissolved in acetone in a two-necked round-bottle flask with magnetic stirrer under nitrogen. The reaction was conducted at 70 °C for 24 h under nitrogen. After polymerization, the product was purified by precipitation from diethyl ether twice to obtained polymers. The poly-dispersity index (PI) was 1.15 from GPC determination using DMSO as an eluted solvent.

2.2. Synthesis of mPEG$_{5000}$-PLA$_{1510}$

mPEG-b-PLA diblock copolymer was also synthesized by ring-opening polymerization [7]. Briefly, mPEG with Mw 5000 and toluene were added to a two necked round-bottle flask with a magnetic stirrer. Stannous octoate was then added to start the polymerization at 130 °C for 16 h under nitrogen. After polymerization the reaction was terminated by adding 0.1N methanolic KOH and the product precipitated from diethyl ether at 0 °C. The polydispersity index (PI) was 1.2 from GPC determination.

2.3. Synthesis of folate-PEG$_{5000}$-PLA$_{1200}$

First, Boc-NH-PEG-PLA diblock copolymer was synthesized by ring opening polymerization from Boc-NH-PEG and lactide using stannous octoate as a catalyst. The Boc-NH-PEG-PLA was then reacted with H$_2$ in the presence of Pd catalyst at room temperature for 24 h to remove Boc. The NH$_2$-PEG-PLA was obtained after filtering out the Pd catalyst and precipitating from ether. Folate-PEG-PLA was prepared in a two step procedure [6]: 1) carboxylation of folic acid with NHS to yield folate-NHS; 2) conjugation of NH$_2$-PEG-PLA with folate NHS at room temperature for 10 h inder nitrogen to produce folate-PEG-PLA. The carbodiimide-activated folic acid can couple with either α or γ carboxyl group residue. Reaction conditions were selected to favor linkage with γ carboxyl residue. The final product was purified by dialysis (dialysis bag with MWCO 2000) against deionized water for 24 h and freeze-dried.

2.4. Synthesis of phenolic ester-PEG$_{5000}$-PLA$_{650}$

First, the hydroxyl end of PLA was synthesized by ring-opening polymerization from N-Boc-L-alaninol and Lactide. The PLA-PEG-COOH was synthesized by DCC-mediated ester coupling reaction using PEG-dicarboxylic acid as a limiting reagent. The product was purified from diethyl ether because the low molecular weight of unreacted PLA could not precipitate in ether. Finally, PLA-PEG-COOH was reacted with hydroquinone by DCC-mediated ester coupling reaction and then precipitated from diethyl ether twice to obtain phenolic ester-PEG-PLA.

2.5. Preparation of Dox-loaded multifunctional hollow nanoparticles

Dox-loaded multifunctional hollow nanoparticles were also prepared by dialysis. The preparation procedure was similar to that of our previous reports [6–9].

Fig. 1. Representation of multifunctional hollow nanoparticle and its TEM image.

Briefly, Dox-HCl, mPEG-PLA, Folate-PEG-PLA, phenolic ester PEG-PLA, and poly(NVI-co-NVP)-g-PLA were dissolved in DMSO. Triethylamine was added in polymer and drug solution to remove hydrochloride. Then, the mixed solution was dialyzed against water at 25 °C for 72 h. The distilled water was replaced every 3 h. After dialysis, the solution of nanoparticles was collected and frozen using a freeze-drying system to yield dried hollow nanoparticles. To measure the drug content of nanoparticles, weighed amounts of the hollow nanoparticles were dissolved in DMSO and then underwent ultrafiltration (ultrafiltration membrane MWCO 10000, Millipore), and samples were removed and analyzed to determine the Dox content using a UV–vis spectrometer at 485 nm, by reference to a calibration curve of Dox in DMSO. The drug content of nanoparticles was calculated using the formula: drug content [% w/w] = (total mass of Dox in nanoparticles)/(total mass of Dox in nanoparticles + total mass of polymer in nanoparticles) × 100.

2.6. Drug release assay

The release behavior of multifunctional hollow nanoparticles loaded with Dox in pH 5.0 and pH 7.4 buffer solutions at 37 °C was determined by measuring, using a UV/Vis spectrometer at 485 nm in a time-course procedure, Dox isolated from a nanoparticle buffer solution (50 mg/l) by ultrafiltration (ultrafiltration membrane MWCO 10000, Millipore).

2.7. Animal studies

Animal care and use was performed in compliance with the "Guide for the Care and Use of Laboratory Animals" prepared by the Institute of Laboratory Animal Resources, National Research Council, and published by the National Academy Press, revised in 1996 and approved by the Institutional Review Board (IRB). For SPECT/CT imaging and biodistribution studies, multifunctional hollow nanoparticles were labeled with ^{123}I on the surface of the phenolic ester-PEG segments using the IodoGen method. Briefly, nanoparticles (10 μL; 25 μg/μL in 0.1 M KH_2PO_4 buffer, pH 7.4) were added into an iodogen precoated tube followed by addition of 10 μL (185 MBq) of Na^{123}I and allowed to incubate at room temperature for 10 min. The labeling efficiency of ^{123}I to nanoparticles was assessed using ascending instant thin layer chromatography (ITLC) with silica gel coated TLC plates (ITLC-SG, PALL Life Sciences, Ann Arbor, MI, USA). ITLC was performed using 85% ethanol in saline as the mobile phase. TLC plates were scanned and analyzed with a Bioscan AR2000 radio-TLC scanner. The results indicated a greater than 90% radiochemical purity.

2.8. SPECT/CT imaging studies

The accumulation of ^{123}I-labeled nanoparticles in cancer tissues was assessed using female Balb-c/nude mice bearing human cervical cancer (HeLa Cells) xenografts. Mice (~20g, 4 weeks) were inoculated in the subcutaneous tissues of the back with 1×10^6 cells/0.1 mL. At 3–4 weeks postinoculation, tumor-bearing mice ($n = 3$; average tumor volume: 120 mm^3) were used in animal imaging experiments. Imaging was performed at a controlled temperature (37 °C) and under anesthesia (1.5% isoflurane in 100% oxygen) using a high-resolution dual modality system (NanoSPECT/CT, Bioscan, Washington DC, USA). Briefly, dynamic scans consisting of 16 frames (30 min per frame) were acquired immediately after injection of ^{123}I-labeled nanoparticles F− or ^{123}I-labeled nanoparticles F+ (120 MBq/0.2 mL) in the tail vein; an additional time frame was acquired at 6 h postinjection. A reference CT scan was performed after SPECT imaging. Coregistered SPECT/CT images were analyzed using the PMOD image analysis software (PMOD Technologies, Zurich, Switzerland). Quantification was performed by volume of interests (VOIs) analysis and expressed as %ID/mL, normalized to the total injected dose. The mean radioactivity within VOIs was converted to % ID/g, under the assumption that 1 mm^3 is equal to 1 mg of tumor or normal tissue.

2.9. Biodistribution

Six tumor-bearing mice (tumor size: 120–130 mm^3) were randomly divided into two groups. Each mouse was injected with 0.2 mL of saline solution containing 1.85 MBq of ^{123}I-labeled nanoparticles F− or ^{123}I-labeled nanoparticles F+ through the tail vein. Animals were then sacrificed by CO_2 inhalation at 6 h postinjection. Blood was withdrawn from the heart through a syringe. Tumor tissues and other organs of interest (i.e., blood, heart, lung, liver, spleen, kidney, muscle, skin, bladder, thyroid and brain) were excised, washed with saline, dried, weighed, and counted on a γ-counter (1470 Wizard, Wallac, Turku, Finland). The organ uptake was calculated as the percentage of the injected dose per gram of wet tissue (% ID/g) using reference counts from a definite sample of the original injectate counted at the same time.

2.10. Ex vivo fluorescence imaging and autoradiography

Tumors and livers were collected, frozen, and embedded in OCT medium (MICROM) immediately after the biodistribution studies. Frozen sections (20 μm in thickness) were prepared in a microtome-cryostat (CM3050S, Leica, Germany). To examine the distribution of Dox in mice, slide-mounted dried specimens were immediately scanned with the FLA-5000 phosphor imager (Fujifilm) at the

following conditions: 473-nm blue light, 700 V, 65,536 tonal gradations and 25-μm resolution. Subsequently, the same sections for ARG were brought into close contact with a BAS-SR 2040 imaging plate (20 × 40 cm, Fujifilm, Japan) and exposed for 24 h in a shield box. After completion of exposure, the plates were scanned with the FLA-5000 phosphor imager (700 V, 65,536 tonal gradations, 25-μm resolution) to reveal the radioactivity distribution in the sections. Images obtained by fluorescence observation and ARG were analyzed using a Multi Gauge version 3.0 software (Fujifilm).

2.11. In vivo antitumor activity

The tumor models were established as described above. When the tumor volume reached approximately 50 mm^3 (7 days after inoculation), animals were randomly divided into two groups (experimental and control groups, six animals per group). Animals were treated i.v. via the tail vein at 4 different time points with an interval of 3 days (days 0, 3, 6 and 9). Mice were injected with 0.2 mL of different formulations of Dox solutions (free Dox, nanoparticles F−, nanoparticles F+, at a dose of 10 mg/kg) or neat saline (negative control). Follow-up was performed for 35 days following the administration experiments were performed. During the course of the follow-up, tumor size was measured three times a week using a Vernier's caliper. Tumor volume was calculated as follows: $V = (ab^2)/2$ (where a and b indicate the major and minor axes of the tumor, respectively). Mice body weight (as an indirect indicator of general animal wellness) and clinical status were carefully recorded. To evaluate the antitumor activity, the relative tumor volume was calculated as the ratio of tumor volume on that day to its value at the start of therapy. To evaluate toxicity, we assessed mortality and relative body weight (calculated as the ratio of tumor volume on that day to its value at the start of therapy). On day 80, mice were sacrificed by CO_2. Blood and tumors were quickly harvested and analyzed.

2.12. TUNEL assay

Excised tumors were immediately embedded into OCT medium and snap frozen in dry ice. 4 mm thick sections were prepared with a cryostat and fixed in 4% paraformaldehyde (EMS, Hatfield, PA) for 20 min at room temperature. After the sections were washed with 0.01 M PBS-Tw (0.3% Tween 20 in PBS at pH = 7.4) three times for 10 min each, the apoptosis cells were stained with ApopTag® Fluorescein In Situ Apoptosis Detection Kit S7110 from Chemicon (Billerica, MA) according to the manufacturer's instruction and the nucleus were labeled with DAPI from KPL (Gaithersburg, MD). The stained tissues were photographed under the Zeiss Axi-oImager Z1 fluorescence microscope system with the automated acquisition system TissueFAXS PlusTM (TissueGnostics, Vienna, Austria) in the same optical and photographical condition. Each tumor area was selected as a ROI for analyzing and quantifying. Individual nuclei in DAPI channel and apoptosis cells in fluorescein channel were recognized and analysis by the algorithms of the TissueQuest (TissueGnostics, Vienna, Austria). The numerical parameters (ex. intensity, area, etc.) were plotted to create Flow Cytometry-like scattergrams. The apoptosis index was calculated by dividing the TUNEL positive cell number by the total cell number (DAPI-positive) within the ROI. All measurements were performed by at least three independent animals in a blind manner.

2.13. Clinical Biochemistry

After a 80-day treatment, blood samples were collected from Balb-c/nude mice and centrifuged at 3000 rpm for 10 min to separate serum from RBCs. Serum was collected in separator tubes and analyzed using the DT60 II and DTSC II modules of the VITROS Chemistry System (Johnson & Johnson, USA). Liver function tests − including aspartate aminotransferase (AST) and alanine aminotransferase (ALT) − and kidney function tests − including blood urea nitrogen (BUN) and creatinine (CRSC) − were carried out using commercially available kits (VITROS AST slide, ALT slide, BUN slide, and CRSC slide; Johnson & Johnson, USA).

3. Results and discussion

3.1. Polymers

In this study, multifunctional hollow nanoparticles consisted of the anticancer drug Dox, a graft copolymer, and three diblock copolymers. Each component performed a specific function in the final micelle, with the ultimate goal of improving tumor-selective delivery of cancer therapeutics. The graft copolymer poly(N-vinylimidazole-co-N-vinylpyrrolidone)-g-poly(D,L-lactide) (P(NVI-co-NVP)$_{9600}$-g-PLA$_{4900}$, [NVI]:[NVP]:[PLA] = 28:69:3) served for encapsulation and storage of the anticancer drug, as well as to control the drug release rate. It was synthesized by the traditional free radical polymerization from the NVI monomer, the NVP

monomer, and the PLA-EMA macromonomer [7–9]. PNVP is water-soluble, carries a net neutral charge, and has excellent biocompatibility properties [12]. When NVI was randomly copolymerized with the graft copolymer, the resulting compound was found to be sensitive to intracellular pH changes (pKa values of NVI around 6.0) in a PNVI chain length-dependent manner [13]. The diblock copolymer, methoxy poly(ethylene glycol)-b-poly(D,L-lactide) (mPEG$_{5000}$-PLA$_{1510}$, [mPEG]:[LA] = 13:87) served as surfactant for controlling micellization and particle size. It was synthesized by ring-opening polymerization [14]. To allow tumor targeting and radiolabeling, two functional end-capped diblock copolymers, folic acid (FA)-PEG$_{5000}$-PLA$_{1200}$ ([PEG]: [LA] = 6:94) and phenolic ester-PEG$_{5000}$-PLA$_{650}$ ([mPEG]:[LA] = 10:90), were synthesized using the N-hydroxysuccinimide (NHS) ester coupling reaction [6] and the DCC-mediated ester coupling reaction, respectively.

3.2. Hollow nanoparticle characterization

For a typical preparation of mixed micelles, doxorubicin hydrochloride was neutralized with a 1.2 molar excess of triethylamine in DMSO [14]. For preparing multifunctional hollow nanoparticles, 17 weight % of graft copolymer, 11 weight % of mPEG-PLA, 17 weight % of FA-PEG-PLA, and 5 weight % of phenolic ester-PEG-PLA were dissolved in the drug solution, followed by dialysis against Milli-Q water for 72 h (membrane molecular weight cutoff: 6000–8000 Da) at room temperature. According to DLS (Malvern, zetasizer 2000) measurements, the particle size was approximately 77.2 nm (intensity average). This size was in keeping to the results of TEM observations. TEM images also provided the direct evidence for observing the hollow structure of spheres. From the results, the TEM images staining 2 wt% uranyl acetate showed that multifunctional hollow nanoparticles were hollow, uniform, and spherical. The hollow structure was perhaps due to the stereorestriction of the pyrrolidine and imidazole rings, resulting in a regular arrangement of graft copolymers. The nanoparticles prepared by graft copolymers alone (see supporting information) similarly displayed hollow cavities. According to UV/VIS spectroscopy, the loading level of Dox from multifunctional hollow nanoparticles dissolved in DMSO was approximately 21% in weight. Multifunctional hollow nanoparticles showed a pulsatile on-off response to pH (Fig. 2a), resulting in an optimal control and timing of drug delivery. The dramatical on/off switch upon changes in pH was due to two opposing forces, i.e. swelling was driven by the protonation of NVIs in acidic surroundings, while deswelling was the result of

hydrophobic PLAs interactions in neutral surroundings. The TEM images (Fig. 2a) showed that the hollow nanoparticle structure was irreversibly destroyed by changes in pH, suggesting a possible dissociation of the diblock copolymers from the nanoparticles structure. However, the on-off release behavior was still preserved. To further elucidate the drug release behavior of multifunctional hollow nanoparticles, we analyzed the drug release dynamics at pH 7.0, 6.5, 6.0 and 5.5. Results (Fig. 2b) showed that, as pH below 6.0, the anticancer drug was rapidly released from multifunctional hollow nanoparticles, followed by a sustained release until a 60 wt% release was reached. The majority of tumors have a vascular pore cutoff size range between 380 and 780 nm [15]. Nanoparticles protected with a large mPEG brush layer with a diameter of 60–100 nm would therefore provide an excellent accumulation in tumor at the blood PK [10]. Of note, a particle size of less than 200 nm is required to avoid spleen filtering effects [16]. Taken together, these results indicate that our multifunctional hollow nanoparticles may ensure a higher intratumoral accumulation of antitumor drugs.

3.3. In vivo biodistribution

We next investigated the *in vivo* biodistribution of multifunctional hollow nanoparticles. Nanoparticles were labeled with ^{123}I on the surface of the phenolic ester-PEG segments using the IodoGen method [17], and subsequently injected via the tail vein into Balb-c/nude mice bearing human cervical cancer HeLa cells. Fig. 3a shows SPECT images of tumor-bearing mouse at various time points following the injection of multifunctional hollow nanoparticles. In the color histogram, different radioactive intensities were represented with the different colors. Results showed that multifunctional hollow nanoparticles (mixed micelles F+) were rapidly distributed through the blood to body tissues. Strong signals were observed in the lung, liver, kidney, and the experimental tumors. Signal intensity in tumors showed a time-dependent effect, suggesting that multifunctional hollow nanoparticles can selectively target tumors through molecular interactions. Comparatively, the signal for nanoparticles without folic acid (mixed micelles F−) was relatively weak in experimental tumors, with striking contrast relative to the liver where high nonspecific accumulation was observed. These results were paralleled by the findings from *in vitro* cytotoxicity assays of multifunctional and normal nanoparticles in HeLa cells (see supporting information).
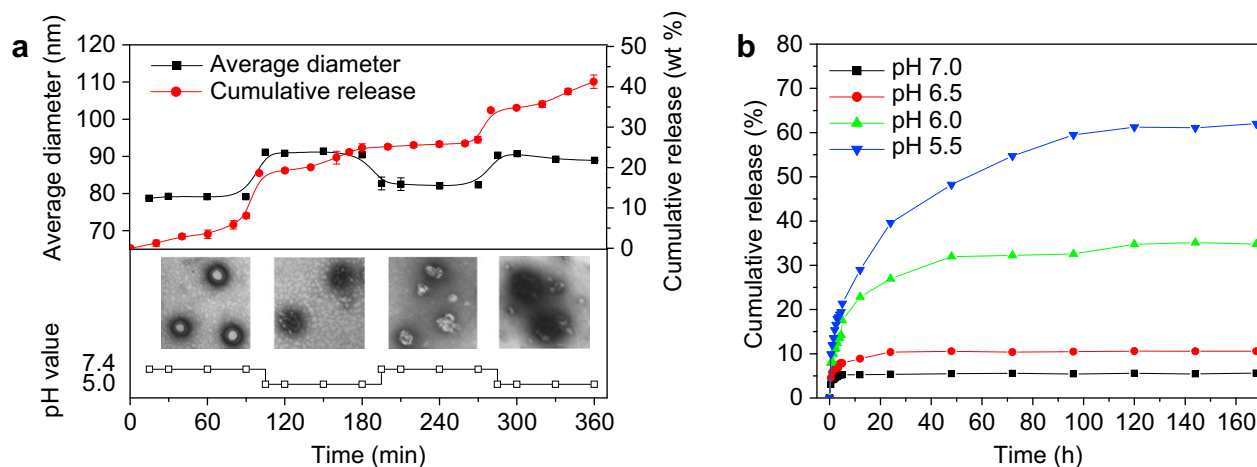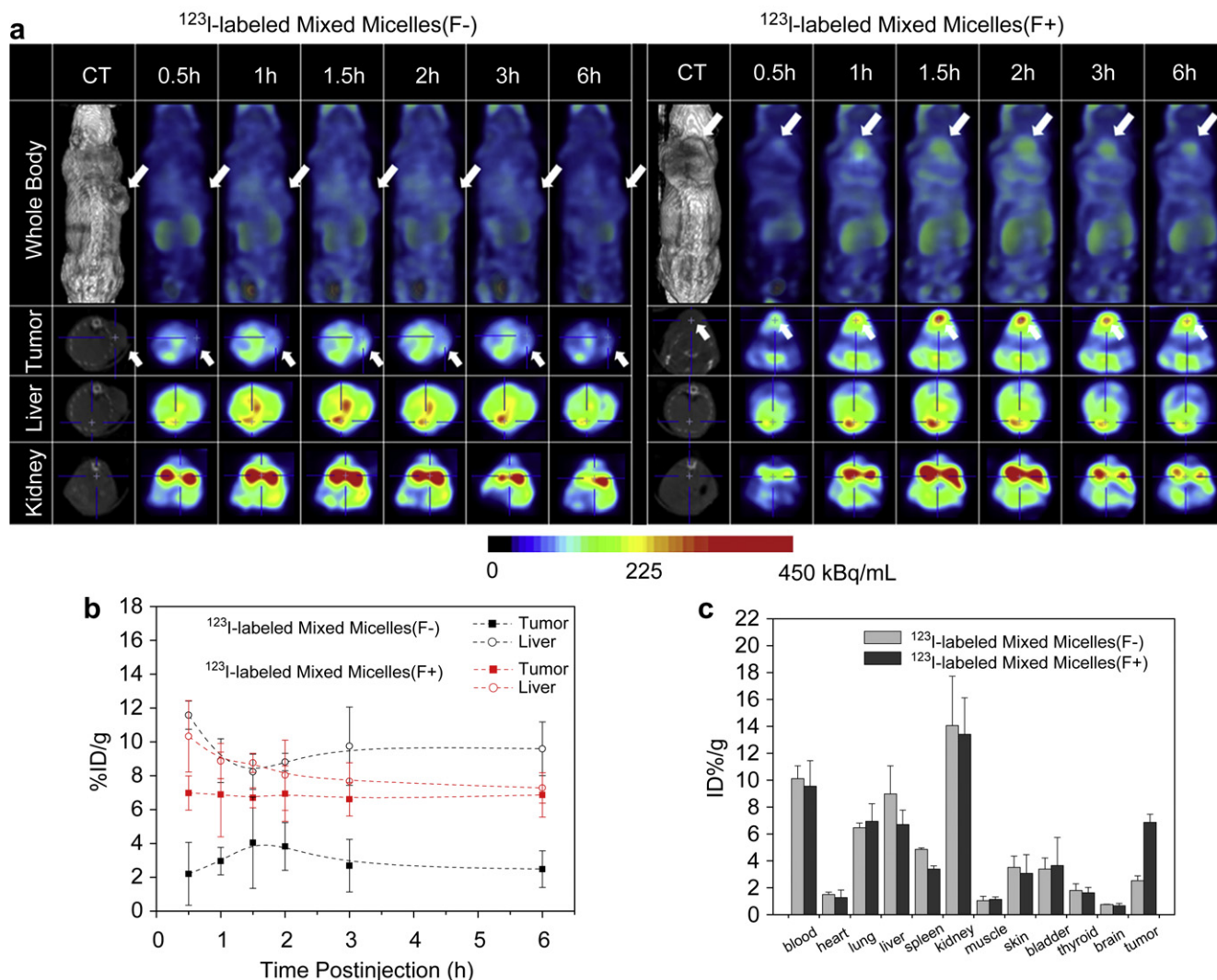

Fig. 2. (a) On-off drug release behavior and corresponding TEM images of multifunctional hollow nanoparticles in response to a change in pH (from 7.4 to 5.0). (b) Dox release from multifunctional hollow nanoparticles under different pH buffer solutions at 37 °C. Data are expressed as means ± SD ($n = 3$).

Fig. 3. (a) SPECT images showing the biodistribution of ^{123}I-labeled nanoparticles (mixed micelles F−) and ^{123}I-labeled multifunctional hollow nanoparticles (mixed micelles F+) in Balb-c/nude mice bearing HeLa tumors. Arrows indicate areas of tumor cell deposit. (b) Radioactivity intensities (volumes of intensity) according to SPECT images in micelles-treated mice allowed the quantification of the nanoparticles accumulation in the liver and tumor tissues. Mean ± SD ($n = 6$). (c) Biodistribution of nanoparticles in major organs of mice at 6 h after intravenous injection. Mean ± SD ($n = 6$).

In order to quantify the radioactivity in the liver and experimental tumors, coregistrated SPECT/CT images were analyzed using the PMOD image analysis software. Fig. 3b shows a high level of tumor radioactivity shortly after administration of multifunctional hollow nanoparticles due to the folate-binding protein (FBP)-binding effect [18]. In addition, experimental tumors showed a moderate level of radioactivity following administration of nanoparticles (mixed micelles F−) with the same particle size. Interestingly, the radioactivity of the tumor tissue increased for 90 min after the administration, and decreased thereafter. Although larger particles (between 40 and 100 nm in size) could have lead to a higher tumor accumulation due to the EPR effect, we hypothesize that the absence of a crowded outer shell of PEG in nanoparticles can result in an increased tissue clearance, ultimately leading to a reduced accumulation. Of note, liver Kupffer cells can rapidly remove particles from the circulation [19], and this may account for the radioactivity signals observed in the liver following the administration of multifunctional and normal nanoparticles. But, a clear drop of radioactivity signal (around 2 %ID/g) in liver with multifunctional nanoparticles treatment was observed because of the active targeting.

At 6 hours postinjection, mice were sacrificed and major organs were harvested to determine the amount of radioactivity from ^{123}I-labeled micelles using a gamma counter [20]. The uptake of nanoparticles by the tumor was 1.96% of the injected dose per gram of tissue (% ID/g) (Fig. 3c). The uptake of nanoparticles into the tumor tripled to 6.3% ID/g in the case of multifunctional hollow nanoparticles. However, the higher accumulations in kidney and bladder were also observed in both multifunctional and normal nanoparticles. These results were in keeping with SPECT findings. It is known that nanocarriers ranging from 10 to 100 nm in size are poorly cleared from the body. They are also unlikely to be cleared via the kidney which has a hydrodynamic diameter cutoff of approximately 6 nm [21]. The high radioactivity in bladder is perhaps due to the dissociation of ^{123}I-labeled-diblock copolymer (with low molecular weight of hydrophobic segment PLA$_{650}$) from nanoparticles following the tumor uptake and then excreted via the kidneys. We can observe that PEG$_{5000}$−PLA$_{650}$ was dissociated from nanoparticles under pH 6.0 buffer solution treatment for 10 min by GPC measurement (see supporting information).

3.4. Ex vivo fluorescence imaging and autoradiography (ARG)

Autoradiography studies [22] clearly showed significant accumulations of nanoparticles and multifunctional hollow nanoparticles in the liver (Fig. 4). However, fluorescence studies suggested the absence of local Dox release of multifunctional hollow nanoparticles. This is perhaps because a portion of radioactivity of multifunctional hollow nanoparticles in the liver was contributed from dissociated ^{123}I-labeled-diblock copolymer. Therefore, Dox fluorescence of multifunctional hollow nanoparticles was non-observable. These results suggest that multifunctional hollow nanoparticles are unlikely to cause significant hepatotoxicity during experimental period of 6 h. In contrast, significant accumulations of radioactivity and fluorescence were found in experimental tumors, suggesting that 1) multifunctional hollow nanoparticles are internalized by cancer cells, and 2) drug release from micelles is triggered by a change in pH.

3.5. In vivo antitumor activity

We next investigated the *in vivo* antitumor efficacy of multifunctional hollow nanoparticles. Balb-c/nude mice bearing human cervical tumors were treated with either free Dox, nanoparticles (mixed micelle F−), or multifunctional hollow nanoparticles (mixed micelle F+). All the treatment modalities were administered by intravenous injection with a frequency of four times at a 3-day interval when the tumors reached a volume of 0.5 cm^3. The growth of subcutaneously-implanted tumors was assessed over a 35-day time frame. Fig. 5A shows that tumor volumes of untreated mice and those treated with free Dox increased very rapidly (13.6- and 12.0-fold increase, respectively). Mice treated with multifunctional hollow nanoparticles also showed some increase (5.1-fold), though the effect was less prominent. These results suggest that multifunctional hollow nanoparticles showed a considerably higher antitumor activity compared with free Dox. This difference may be attributed to the high affinity FBP-binding effect. To evaluate the cytotoxicity of multifunctional hollow nanoparticles, the body weight of mice was measured in each treatment arm. Fig. 5b shows that mice treated with free Dox at a concentration of 5 mg/kg exhibited a 12% decrease of body weight within 10 days (4 injections), and appeared to be weak after treatment. The main side effects associated with treatment with free Dox include leukopenia as well as cardiac, hepatic, and renal injury [23−25]. In our study, treatment with multifunctional hollow nanoparticles resulted in a minimal weight loss (approximately 5%), suggesting that this drug carrier may significantly reduce Dox toxicity to normal tissues.

3.6. Tumor apoptosis

We next assessed tumor apoptosis (from biopsy specimens obtained from the middle of the lesion) revealed by TUNEL staining [26] after 80 days of treatment with multifunctional hollow nanoparticles. In addition, DAPI (4′,6-diamidino-2-phenylindole) was used to stain nuclei of tumor cells. Specimens treated with DAPI alone served as negative control (Fig. 6). Results showed that both free Dox and nanoparticles (mixed micelles F−) did not induce significant apoptosis of tumor cells above the control level. On the other hand, multifunctional hollow nanoparticles (mixed micelles F+) induced higher rates of apoptosis in tumor cells as measured by TUNEL assay (approximately 34.3%). These pilot data clearly indicate that multifunctional hollow nanoparticles provide a higher therapeutic efficacy compared with the free drug or other micelles [27,28].

3.7. Clinical Biochemistry

We finally asked whether long-term treatment with multifunctional hollow nanoparticles may induce hepatic or renal toxicity. We therefore analyzed serum biomarkers of liver and kidney function in the three study arms (free Dox, nanoparticles, multifunctional hollow nanoparticles) following a 80-day treatment course. AST, ALT, BUN, and CRSC were measured in all animals. Normal reference values for AST, ALT, BUN, and CRSC in mice are 28−132 U/L, 59−247 U/L, 18−29 mg/dL, and 0.2−0.8 mg/dL, respectively. Fig. 7 shows that treatment with either nanoparticles (mixed micelles F−) or multifunctional hollow nanoparticles (mixed micelles F+) did not increase ALT, BUN, AST, or CRSC levels beyond normal values. These results suggest that long-term treatment with micelles does not appreciably alter liver or kidney function in our mouse model. Of note, high AST levels were evident in free Dox-treated animals as well as in the untreated control group. AST is a marker of liver cytolysis, but elevations of the AST level may also be seen in heart, kidney, muscles, or brain injury. AST elevation in Dox-treated mice suggests cardiac injury, and it is widely known that Dox may exert deleterious effects on heart tissue [29]. Otherwise, high level of AST for control group is due to the human cervical tumors implanted in mice [30].
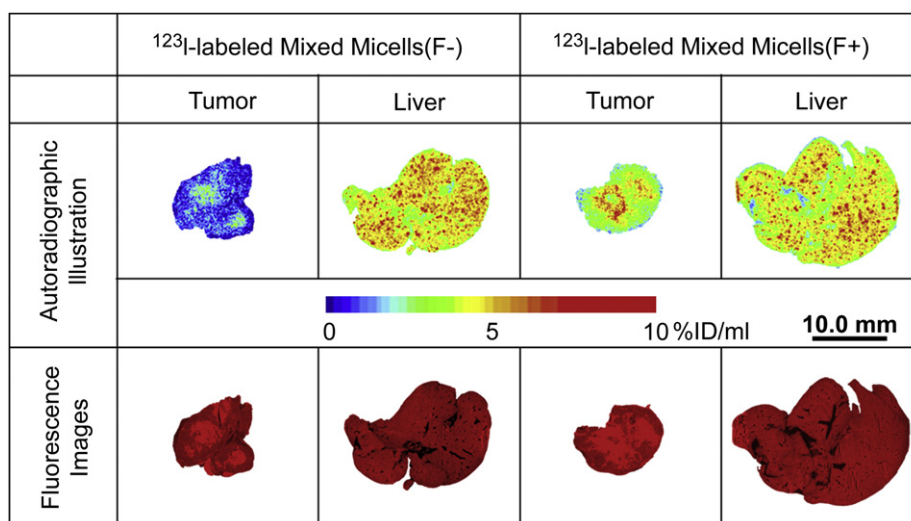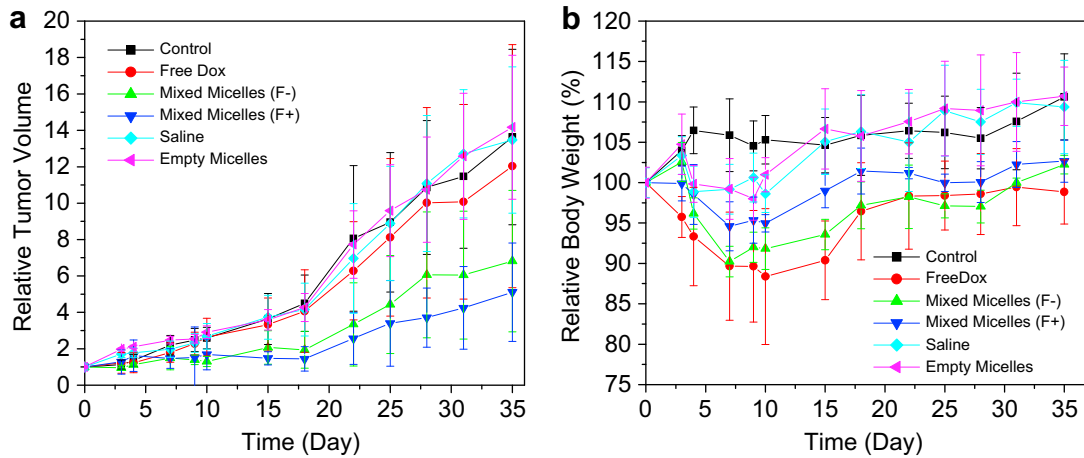

Fig. 4. Autoradiographic detection and fluorescence images of mouse liver and tumor at 6 h after intravenous injection of nanoparticles allowed the evaluation of the *in vivo* stability of nanoparticles.

Fig. 5. (a) *In vivo* anticancer efficacy and (b) body weight changes in Balb-c/nude mice bearing HeLa tumors after intravenous administration of free Dox, nanoparticles (mixed micelles F−), and multifunctional hollow nanoparticles (mixed micelles F+) at a 5 kg/mg Dox equivalent dose. Mice were treated with either free Dox or nanoparticles intravenously for four times at a 3-day time interval. Data are expressed as means ± SD ($n = 6$).

3.8. Advantages and possible reasons of multifunctional hollow nanoparticles for high tumor inhibition and low side effects

To our knowledge, this study provides the first example of on-off switched multifunctional hollow nanoparticles prepared using a graft-diblock copolymer-mixed micelle system. This approach offers great promise for new drug delivery options and *in vivo* imaging in the field of oncology. This system offers the features and advantages of both nanoparticles and hollow nanoparticles. Accordingly, multifunctional hollow nanoparticles may be easily prepared at a specific particle size distribution using a dialysis method. Such nanoparticles allow imaging, targeting, and treating the tumor and can be successfully assembled by simple mixing of two or more copolymers. They can encapsulate therapeutic agents
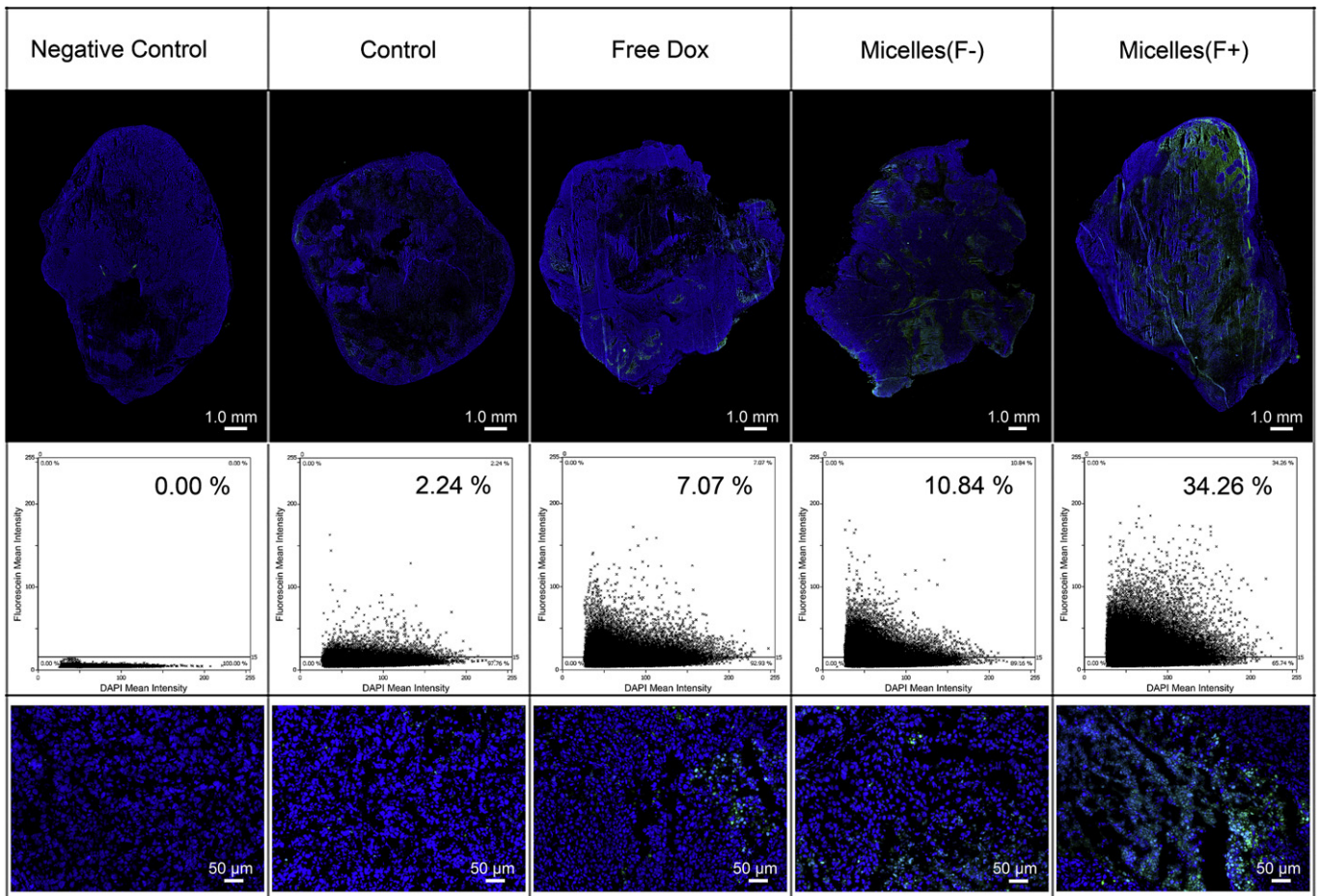
Fig. 6. TUNEL apoptotic cell detection in tumor-bearing mice following a 80-day treatment course. Green: apoptotic cells; blue: DAPI. Upper: whole tumor section; Middle: Apoptosis index (Mean ± SD ($n = 3$)); Lower: tumor cell.
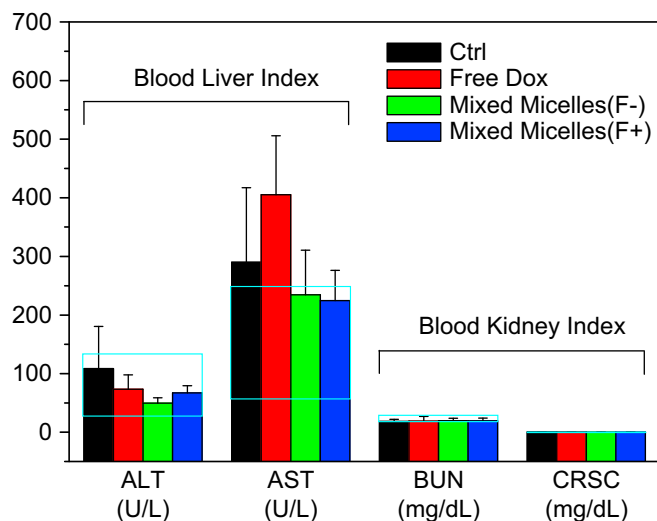
Fig. 7. Changes in biochemical markers of liver and kidney function following a 80-day treatment course. Measurements were carried out with the aim of evaluating the potential long-term toxicity of remnant nanoparticles, polymers and drugs. Mean ± SD ($n = 3$).

or contrast media in the bilayer structure between the lipophilic regions or in their hollow cavity according to the polarity of the encapsulated active agents.

The results of this study indicate that multifunctional hollow nanoparticles exhibit rapid drug release and an excellent antitumor activity. Several reasons may explain these positive findings. The physical properties of microparticles have been shown to play a pivotal role in influencing *in vivo* phagocytosis [31] and clearance from the circulation [32]. Multifunctional hollow nanoparticles have a small size and a flexible and hollow structure. In addition, they contain a cancer-targeting ligand that dramatically reduces their clearance by macrophages while increasing accumulation at tumor sites. Thus far no studies have examined the effects of drug carriers on the therapeutic efficacy of anticancer drugs. It is feasible to hypothesize, however, that the initial rapidly delivery of the therapeutic compound may improve the clinical outcomes. In this study, the rapid NVIs response resulted in a dissociation of the diblock copolymers from nanoparticles, followed by a rapid on-off switching drug release. These findings indicate that multifunctional hollow nanoparticles can enable and augment targeted drug delivery to tumors. Although the hollow structure of multifunctional hollow nanoparticles were destroyed by the change in intracellular pH, the drug may remain tightly bound to their hydrophobic regions, thus preventing or decreasing the leakage of the anticancer drug to systemic circulation or its uptake by the reticuloendothelial system.

4. Conclusions

We have described the preparation of hollow multifunctional hollow nanoparticles that may be obtained through the simple mix of four functional copolymers. All materials used in this study were relatively safe and highly sensitive to intracellular pH changes. The shape and size of micelles were suitable for successful drug delivery under physiological conditions. *In vivo* experiments clearly showed that animals treated with multifunctional hollow nanoparticles exhibited a significantly higher tumor growth inhibition, without signs of liver and kidney damage. It appears that multifunctional hollow nanoparticles hold great potential to use in cancer therapy.

Appendix

Figure with essential color discrimination. Figs. 2, 5 and 7 in this article have parts that are difficult to interpret in black and white. Supplementary data associated with this article can be found, in the online version, at doi:10.1016/j.biomaterials.2010.11.051.

References

[1] Duncan R. Polymer conjugates as anticancer nanomedicines. Nat Rev Cancer 2006;6:688–701.
[2] Seymour LW, Ferry DR, Anderson D, Hesslewood S, Julyan PJ, Poyner R, et al. Hepatic drug targeting: phase I evaluation of polymer bound doxorubicin. J Clin Oncol 2002;20:1668–76.
[3] Low PS, Antony AC. Folate receptor-targeted drugs for cancer and inflammatory diseases. Adv Drug Deliv Rev 2004;56:1055–8.
[4] Bae Y, Nishiyama N, Kataoka K. In vivo antitumor activity of the folate-conjugated pH-sensitive polymeric micelle selectively releasing adriamycin in the intracellular acidic compartments. Bioconjug Chem 2007;18:1131–9.
[5] Kim D, Gao ZG, Lee ES, Bae YH. In vivo evaluation of doxorubicin-loaded polymeric micelles targeting folate receptors and early endosomal pH in drug-resistant ovarian cancer. Mol Pharm 2009;6:1353–62.
[6] Tsai HC, Chang WH, Lo CL, Tsai CH, Chang CH, Ou TW, et al. Graft and diblock copolymer multifunctional micelles for cancer chemotherapy and imaging. Biomaterials 2010;31:2293–301.
[7] Lo CL, Huang CK, Lin KM, Hsiue GH. Self-assembly of a micelle structure from graft and diblock copolymers: an Example of overcoming the limitations of polyions in drug delivery. Adv Funct Mater 2006;16:2309–16.
[8] Huang CK, Lo CL, Chen HH, Hsiue GH. Multifunctional micelles for cancer cell targeting, distribution imaging, and anticancer drug delivery. Adv Funct Mater 2007;17:2291–7.
[9] Lo CL, Huang CK, Lin KM, Hsiue GH. Mixed micelles formed from graft and diblock copolymers for application in intracellular drug delivery. Biomaterials 2007;28:1225–35.
[10] Chithrani BD, Ghazani AA, Chan WCW. Determining the size and shape dependence of gold nanoparticle uptake into mammalian cells. Nano Lett 2006;6:662–8.
[11] Jiang W, Kim BYS, Rutka JT, Chan WCW. Nanoparticle-mediated cellular response is size-dependent. Nat Nanotechnol 2008;3:145–50.
[12] Park IK, Ihm JE, Park YH, Choi YJ, Kim SI, Akaike T, et al. Galactosylated chitosan (GC)-graft-poly(vinyl pyrrolidone) (PVP) as hepatocyte-targeting DNA carrier. Preparation and physicochemical characterization of GC-graft-PVP/DNA complex (1). J Control Release 2003;86:349–59.
[13] Molina MJ, Gómez-Antón MR, Piérola IF. Factors driving protonation of poly (N-vinylimidazole) hydrogels. J Polym Sci Part B Polym Phys 2004;42:2294–307.
[14] Soppimath KS, Tan DCW, Yang YY. pH-triggered thermally responsive polymer core-shell nanoparticles for drug delivery. Adv Mater 2005;17:318–20.
[15] Hobbs SK, Monsky WL, Yuan F, Gregory Roberts W, Griffith L, Torchilin VP, et al. Regulation of transport pathways in tumor vessels: role of tumor type and microenvironment. Proc Natl Acad Sci USA 1998;95:4607–12.
[16] Moghimi SM, Porter CJH, Muir IS, Illum L, David SS. Non-phagocytic uptake of intravenously injected microspheres in rat spleen: influence of particle size and hydrophilic coating. Biochem Biophys Res Commun 1991;177:861–6.
[17] Schottelius M, Wester HJ, Reubi JC, Senekowitsch-Schmidtke R, Schwaiger M. Improvement of pharmacokinetics of radioiodinated Tyr(3)-octreotide by conjugation with carbohydrates. Bioconjug Chem 2002;13:1021–30.
[18] Elwood PC. Molecular cloning and characterization of the human folate-binding protein cDNA from placenta and malignant tissue culture (KB) cells. J Biol Chem 1989;264:14893–901.
[19] Ferrucci JT, Stark DD. Iron oxide-enhanced MR imaging of the liver and spleen: review of the first 5 years. Am J Roentgenol 1990;155:943–50.
[20] Choi HS, Itty Ipe B, Misra P, Lee JH, Bawendi MG, Frangioni JV. Tissue- and organ-selective biodistribution of NIR fluorescent quantum dots. Nano Lett 2009;9:2354–9.
[21] Choi HS, Liu W, Misra P, Tanaka E, Zimmer JP, Itty Ipe B, et al. Renal clearance of quantum dots. Nat Biotechnol 2007;10:1165–70.

[22] Lin KJ, Ye XX, Yen TC, Wey SP, Tzen KY, Ting G, et al. Biodistribution study of [(123)I] ADAM in mice: correlation with whole body autoradiography. Nucl Med Biol 2002;29:643–50.

[23] Zeidan Q, Strauss M, Porras N, Anselmi G. Differential long-term subcellular responses in heart and liver to adriamycin stress. Exogenous L-carnitine cardiac and hepatic protection. J Submicrosc Cytol Pathol 2002;34:315–21.

[24] Di Donato A, Ghiggeri GM, Di DM, Jivotenko E, Acinni R, Campolo J. Lysyl oxidase expression and collagen cross-linking during chronic adriamycin nephropathy. Nephron 1997;76:192–200.

[25] Singal PK, Deally CM, Weinberg LE. Subcellular effects of adriamycin in the heart: a concise review. J Mol Cell Cardiol 1987;19:817–28.

[26] Doronina SO, Mendelsohn BA, Bovee TD, Cerveny CG, Alley SC, Meyer DL, et al. Enhanced activity of monomethylauristatin F through monoclonal antibody delivery: effects of linker technology on efficacy and toxicity. Bioconjug Chem 2006;17:114–24.

[27] Wu XL, Kim JH, Koo H, Bae SM, Shin H, Kim MS, et al. Tumor-targeting peptide conjugated pH-responsive micelles as a potential drug carrier for cancer therapy. Bioconjug Chem 2010;21:208–13.

[28] Ko YT, Falcao C, Torchilin VP. Cationic liposomes loaded with proapoptotic peptide D-(KLAKLAK)(2) and Bcl-2 antisense oligodeoxynucleotide G3139 for enhanced anticancer therapy. Mol Pharm 2009;6:971–7.

[29] Licate S, Saponiero A, Mordente A, Minotti G. Doxorubicin metabolism and toxicity in human myocardium: role of cytoplasmic deglycosidation and carbonyl reduction. Chem Res Toxicol 2000;13:414–20.

[30] Manju V, Balasubramanian V, Nalini N. Oxidative stress and tumor markers in cervical cancer patients. J Biochem Mol Biol Biophys 2002;6:387–90.

[31] Beningo KA, Wang YL. Fc-receptor-mediated phagocytosis is regulated by mechanical properties of the target. J Cell Sci 2002;115:849–56.

[32] Geng Y, Dalhaimer P, Cai SS, Tsai R, Tewari M, Minko T, et al. Shape effects of filaments versus spherical particles in flow and drug delivery. Nat Nanotechnol 2007;2:249–55.